Applied Geochemistry 31 (2013) 119–132

Contents lists available at SciVerse ScienceDirect

Applied Geochemistry

journal homepage: www.elsevier.com/locate/apgeochem

Delineating mineralized phases based on lithogeochemical data using multifractal model in Touzlar epithermal Au–Ag (Cu) deposit, NW Iran

Seyed Mehran Heidari [a], Majid Ghaderi [a,*], Peyman Afzal [b]

[a] Department of Economic Geology, Tarbiat Modares University, Tehran, Iran
[b] Department of Mining Engineering, South Tehran Branch, Islamic Azad University, Tehran, Iran

ARTICLE INFO

Article history:
Received 2 July 2011
Accepted 20 December 2012
Available online 31 January 2013
Editorial handling by A. Danielsson

ABSTRACT

The aim of this study is to delineate and separate mineralization phases based on surface lithogeochemical Au, Ag, As and Cu data, using the Concentration–Area (C–A) fractal method in the Touzlar epithermal Au–Ag (Cu) deposit, NW Iran. Four mineralization phases delineated by multifractal modeling for these elements are correlated with the findings of mineralization phases from geological studies. The extreme phase of Au mineralization is higher than 3.38 ppm, which is correlated with the main sulfidation phase, whereas Ag extreme phase (higher than 52.48 ppm) is associated with silicic veins and veinlets. The resulting multifractal modeling illustrates that Au and Ag have two different mineralization trends in this area. Extreme (higher than 398.1 ppm) and high mineralization phases of Cu from the C–A method correlate with hydrothermal breccias and main sulfidation stage in the deposit, respectively. Different stages of Au mineralization have relationships with As enrichment, especially in high and extreme (higher than 7.9%) phases. The obtained results were compared with fault distribution patterns, showing a positive correlation between mineralization phases and the faults present in the deposit. Moreover, mineralization phases of these elements demonstrate a good correlation with silicification and silicic veins and veinlets.

1. Introduction

Study of mineralogy and paragenetic sequence provides useful data on ore-forming processes in deposits in a way that characteristics of different types of deposits exist in their mineral assemblages (Craig and Vaughan, 1994). Therefore, delineation and separation of mineralization phases are two important tasks in economic geology studies as well as mineral exploration. Among different types of deposits, separation of mineralization is difficult in epithermal precious-metal deposits due to close relation between alteration and mineralization. These deposits are very important, because they produce a great proportion of gold and silver throughout the world (Hedenquist et al., 2000). Mineralogical and geochemical characteristics are the basis for separation of mineralization phases in epithermal deposits (e.g., Pirajno, 1992; Richards, 1995; White and Hedenquist, 1995; Sillitoe, 1997; Hedenquist et al., 2000; Jensen and Barton, 2000; Pirajno and Bagas, 2002; Chouinard et al., 2005; Hoefs, 2009). Classical methods are based on mineralographical and petrographical studies including alteration assemblage and ore mineral identification using X-ray Diffraction (XRD), Electron Probe Micro Analyzer (EPMA), Scanning Electron Microscopy (SEM) and Portable Infrared Mineral Analyzer (PIMA) (Hudson, 2003; San Shen and Yang, 2004; Chouinard et al., 2005; Hoefs, 2009). Fluid inclusion and stable isotope studies are other methods for delineating different mineralization phases based on thermometric and isotope element parameters within other geological characteristics (e.g., Faure et al., 2002; Boyce et al., 2007).

Fractal geometry established by Mandelbrot (1983) is a non-linear geometry based on the Latin word "fractus" and has been widely applied in geosciences (e.g., Turcotte, 1986; Meng and Zhao, 1991; Agterberg et al., 1993, 1996; Cheng et al., 1994; Goncalves et al., 1998; Cheng, 1999; Sim et al., 1999; Davis, 2002; Shen and Zhao, 2002; Li et al., 2003; Ali et al., 2007; Carranza, 2009; Zuo et al., 2009a,b,c,d; Afzal et al., 2010; Carranza and Sadeghi, 2010; Zuo, 2011a,b). Cheng et al. (1994) proposed the Concentration–Area (C–A) fractal method for separating different geochemical populations especially for hydrothermal deposits. This method has been an evolution in geochemical studies for recognition of different grade anomalies and related mineralization from background. Fractal dimensions in geological and geochemical processes correspond to variations in physical attributes such as rock type, vein density or orientation, fluid phase, alteration phenomena, structural feature or dominant mineralogy, and so on (Sim et al., 1999). It has been revealed that hydrothermal mineral deposits, such as epithermal Au–Ag (Cu) deposits, present non-Euclidean variations in ore element concentrations in rocks

* Corresponding author. Tel./fax: +98 21 82884406.
E-mail address: mghaderi@modares.ac.ir (M. Ghaderi).

0883-2927/$ - see front matter © 2013 Elsevier Ltd. All rights reserved.
http://dx.doi.org/10.1016/j.apgeochem.2012.12.014

and related surface materials such as water, soil, stream sediment, till, humus, and vegetation (Cheng et al., 1994; Cheng, 2007; Cheng and Agterberg, 2009). Carranza (2008, 2009) proposed a conceptual model of district-scale mechanism of geologic controls on low-sulfidation epithermal Au mineralization based on fractal and fry analysis.

Therefore, fractal dimensions of variations in geochemical data can provide useful information and applicable criteria to separate and delineate mineralization phases within an epithermal system. Various log–log plots in fractal methods are proper tools for separating geological recognition and separation of populations based on geochemical data because threshold values can be recognized, determined and indicated as breakpoints in those plots. These geochemical threshold values are recognized although fractal analyses usually correlate with geological field observation features or processes (Afzal et al., 2011). Fractal/multifractal models consist of the frequency distribution and the spatial self-similar characteristics of geochemical variables, and have been demonstrated to be effective instruments for decomposing geological complexes and mixed geochemical populations and to identify weak geochemical anomalies hidden within strong geochemical background (Cheng, 2007; Cheng and Agterberg, 2009; Zuo, 2011a). However, some resulted breakpoints in fractal modeling may be noises caused by random or calculated errors but these modelings are effective for finding different ore mineralization phases in various ore deposit types.

The main aim of this paper is to recognize and delineate different mineralization phases based on C–A fractal method in the Touzlar Au–Ag (Cu) epithermal deposit, NW Iran. Multifractal modeling for Au, Ag, As and Cu is performed for separation of sulfide mineralization according to lithogeochemical sample analysis and correlated with geological characteristics in this deposit.

2. Concentration–Area fractal method

Cheng et al. (1994) proposed the concentration–area (C–A) method, which may be used to define the geochemical background and different anomalies, as the following form:

$$A(\rho \leqslant \upsilon) \infty \rho^{-a1}; \quad A(\rho \geqslant \upsilon) \infty \rho^{-a2} \tag{1}$$

where $A(\rho)$ denotes the area with concentration values greater than the contour value ρ; υ represents the threshold; and a_1 and a_2 are characteristic exponents. The two approaches used to calculate $A(\rho)$ by Cheng et al. (1994) were: (1) The $A(\rho)$ which is the area enclosed by contour level ρ on a geochemical contour map resulting from interpolation of the original data using a weighted moving average method, and (2) $A(\rho)$ that are the values obtained by box-counting of original elemental concentration values. By box counting, one superimposes grid with cells on the study region. The area $A(\rho)$ for a given ρ is equal to the number of cells multiplied by cell area with concentration values greater than ρ. The breaks between straight-line segments on this plot and the corresponding values of ρ have been used as cut-offs to separate geochemical values into different components, at the same time representing different causal factors, such as lithological differences and geochemical processes. Factors such as mineralizing events, surficial geochemical element concentrations and surficial weathering are important to be considered (Goncalves et al., 2001; Lima et al., 2003).

Multifractal theory may be interpreted as a theoretical framework that explains the power-law relations between areas enclosing concentrations below a given value and the actual concentrations themselves. To illustrate and prove if data distribution has a multifractal nature, a rather extensive computation is required (e.g., Halsey et al., 1986; Evertz and Mandelbrot, 1992; Lima et al., 2003; Afzal et al., 2010). The C–A method seems to be equally applicable to all cases as well, which is probably rooted in the fact that geochemical distributions satisfy mostly the properties of a multifractal function. Some approaches seem to support the idea that geochemical data distributions are multifractal (Bolviken et al., 1992; Cheng and Agterberg, 1996; Goncalves et al., 2001). This idea may provide the development of an alternative interpretation validation and useful methods, which could be applied to elemental geochemical distribution analysis and related mineralization.

3. Geological setting of Touzlar deposit

3.1. Regional geology

The Touzlar epithermal Au–Ag (Cu) deposit, NW Iran, is located about 30 km NW of the city of Mahneshan in Takab magmatic complex, as illustrated in Fig. 1. This complex, with E–W to NW trending, is a part of the Sahand–Bazman Cenozoic magmatic arc (SBCMA), which crosscuts northeastern rim of Sanandaj–Sirjan zone in the Zagros orogeny (Fig. 1). This magmatic arc, in fact is a part of Alpine orogenic belt that is related to Neothetys subduction (Stocklin, 1968; Berberian and King, 1981; Berberian et al., 1982; Hassanzadeh, 1993; Alavi, 1994, 2004; Glennie, 2000; Agard et al., 2005; Shahabpour, 2005; Allen et al., 2006; Ghasemi and Talbot, 2006). Therefore, geodynamic setting of the area is an active continental margin, providing a suitable geological environment for forming epithermal related to alkaline and calc–alkaline magmatism and orogenic gold deposits (Cooke and Simmons, 2000; Hedenquist et al., 2000; Sillitoe, 2002; Groves et al., 2005; Robb, 2005; Simmons et al., 2005; Goldfarb et al., 2007; Groves and Bierlein, 2007). Some of the main gold deposits in Iran are related to Zagros orogeny, specifically in Sanandaj–Sirjan zone as well as Sahand–Bazman Cenozoic magmatic arc which have been active since Jurassic–Cretaceous (e.g., Berberian and King, 1981; Hassanzadeh, 1993; Alavi, 1994, 2004; Shahabpour, 2005; Ghasemi and Talbot, 2006; Shafiei et al., 2009).

Most lithology outcrop units in the area include Neoproterozoic metamorphic rocks (Hassanzadeh et al., 2008) called basement rocks, Paleozoic–Mesozoic, mostly Permian–Upper Triassic and Jurassic–Cretaceous sediments and Cenozoic sedimentary and volcanic-intrusive units, but these units have been covered by Quaternary alluvium and travertine (Alavi et al., 1982). Most of outcrop units in the area are intruded by Tertiary volcanics, which in depth are connected to the subvolcanic intrusive body that cuts the metamorphic rocks. The most significant obvious mineralization in the area is gold mineralization with Miocene volcanics and subvolcanic rocks. In this area, there are two distinguishable types of gold mineralization, including epithermal type related to shallow intrusive body such as Sari Gunay Au–As–Sb deposit (Richards et al., 2006) and sedimentary-hosted gold mineralization type such as Zarshuran and Aghdarreh deposits (Mehrabi et al., 1999; Asadi Haroni et al., 2000; Daliran et al., 2002; Daliran, 2007). Among them, the magmatic system in which the Touzlar deposit is hosted, is composed of pyroclastic, lava flow sequences that have been intruded by microdiorite porphyritic stocks. This complex is residual of an eroded stratovolcano which is highly potassic calc–alkaline to mildly alkaline especially shoshonitic in composition (Amidi et al., 1984; Kazmin et al., 1986; Aftabi and Atapour, 2000; Emami, 2000; Richards et al., 2006).

3.2. Mineralization phases in Touzlar deposit

Hydrothermal activity in the Touzlar Au–Ag (Cu) deposit is related to subvolcanic rocks and covers an area of about 6 km^2 with EEN–WWS trend, as illustrated in Fig. 1. The inner alteration zone is characterized by silicic veins. The intermediate alteration zone

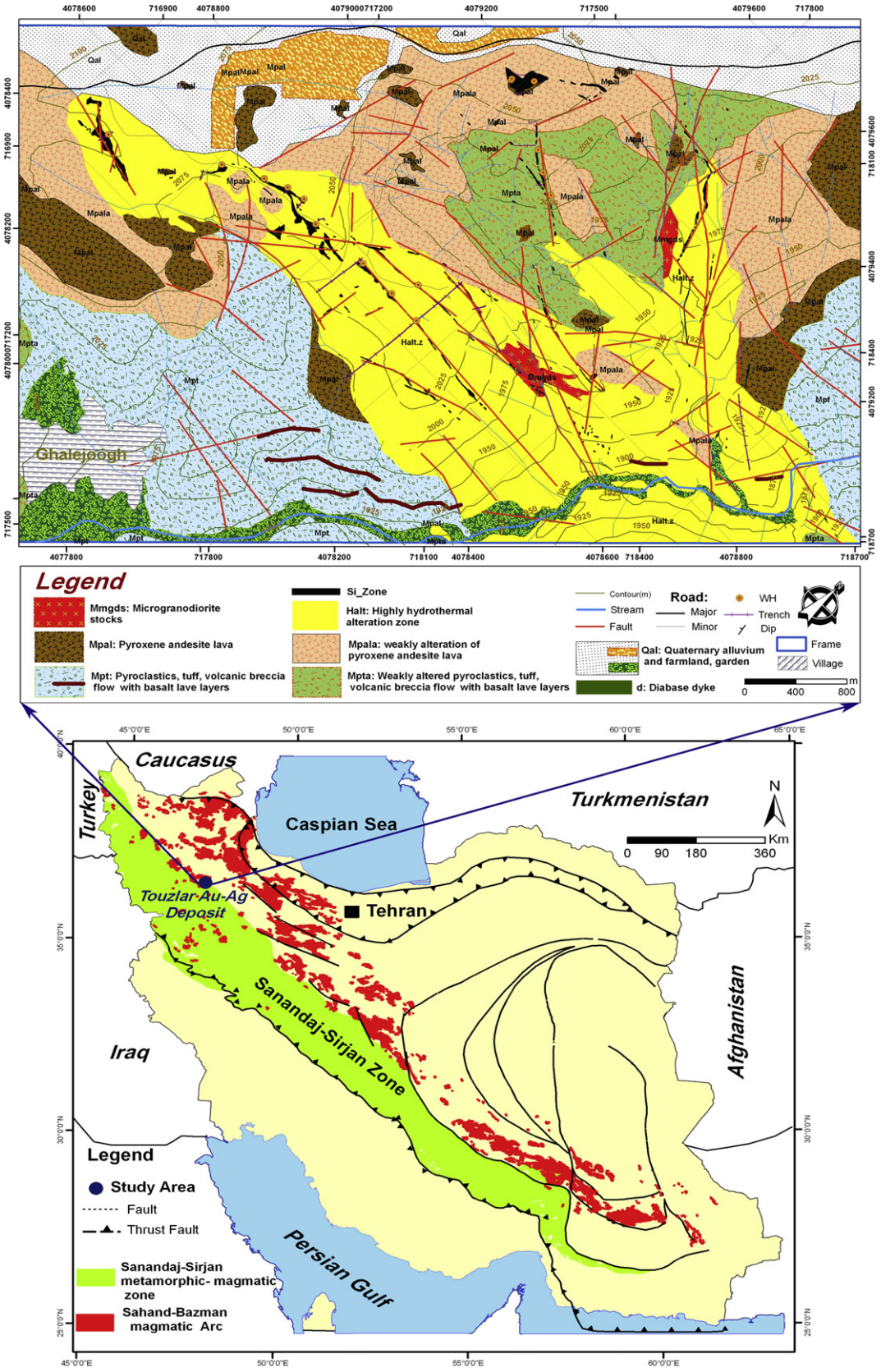

Fig. 1. Geology of Iran showing the location of study area in metamorphic–magmatic Sanandaj–Sirjan zone, and Sahand–Bazman magmatic arc (compiled and simplified by Sahandi et al. (2005), Based on the 1:2,500,000 geologic map of Iran), the geological map of the Touzlar deposit (modified after Rabiei et al. (2006)) and location map of lithogeochemical samples in Touzlar deposit.

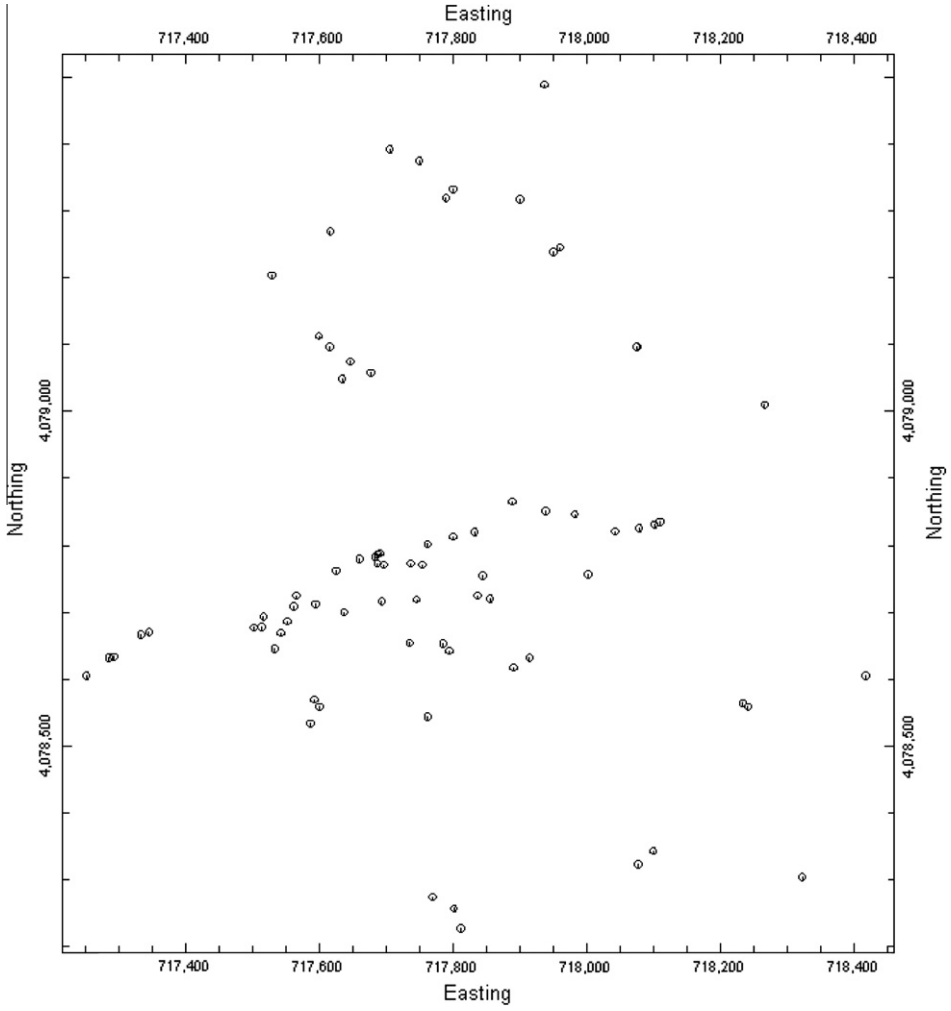

Fig. 1. (*continued*)

Table 1
Evolution stages and phases of mineralization in Touzlar deposit.

	Hydrothermal alteration				
Mineralization	Pre-mineralization	Mineralization			
Evolution stages	Stage 1	Stage 2		Stage 3	Stage 4
Mineralization phases	–	Ph. I	Ph. II	Ph. III	Ph. IV
Alteration minerals (XRD)	Quartz, sericite, clay minerals, carbonate, chlorite, epidote, illite, montmorillonite, sulfide		Quartz, sericite, clay minerals, alunite, illite, montmorillonite, sulfide	Quartz, sulfide	Quartz, sulfide, sericite, barite, fluorite

has different intensities of argillic alteration. The outer alteration zone is distinguished by a vast propylitic alteration. Based on the field geology, mineralographical as well as EPMA and XRD studies, evolution of the system comprises of four stages of mineralization that have occurred in four phases (Table 1).

The pre-mineralization stage in Touzlar gold deposit has formed residual silica cap by argillic alteration during primary phases of epithermal-porphyry systems (Sillitoe, 1997, 2002; Pirajno, 2009). This silica belongs to host rocks, which are influenced by acidic fluid leaching and intense silicification with vuggy quartz textures that are locally preserved in this zone. Average contents of precious metal and associated base metal mineralization in this stage are very low and similar to the host rocks.

The second stage of hydrothermal system accompanies the mineralization and is related to silicification that occurs in the form of replacement in fracture zones. This stage is related to influx of siliceous hydrothermal fluids in the parts that have more permeability and are composed of two phases. Phase I of mineralization is the most abundant, widespread in silicification zone of the deposit. This phase is characterized by bright (white), fine grains of quartz (higher than 90%), leucoxene and low contents of sulfide (<1–2%) mainly including pyrite, arsenian pyrite and native sulfur. High amounts of As-bearing minerals exist in this phase. Grades of gold mineralization in this phase are very low and maximum accede to 100–200 ppb. In contrast, phase II of this stage is characterized by more sulfides in lower volume of silica compared to phase I. The sulfide content in this phase reaches 2–3% and includes pyrite and low amounts of arsenopyrite, galena, sphalerite and chalcopyrite. Average gold content in this phase is <1 ppm occurring as solid solution within the sulfides. Silver grade in this stage is very high and has a

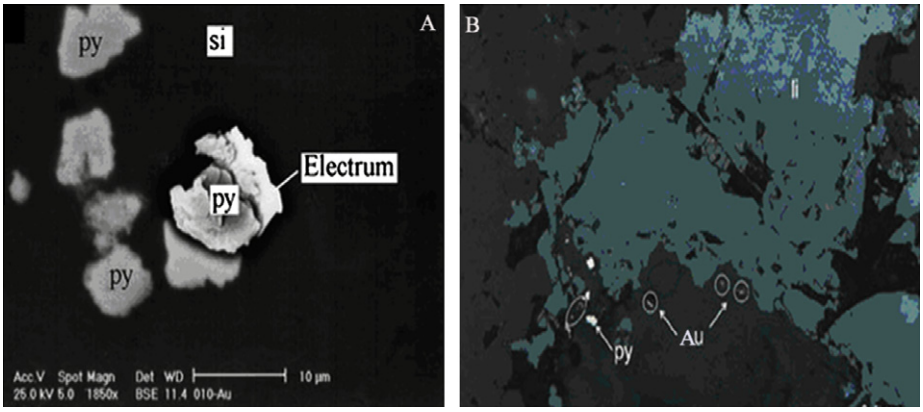

Fig. 2. Grains of gold (Au) in quartz related to third phase of mineralization indicated by SEM (Rabiei et al., 2006).

high correlation with lead, which is due to presence of argentite in galena (Ag/Au greater than 1).

The third stage is another phase of silicic alteration existing in form of crosscutting veins, veinlets and hydrothermal breccias in the silicified zone. Hydrothermal breccias in this stage contain silicified alteration fragments (phases I and II), which are filled by matrix of silica and sulfide. Sulfides are quite abundant in this phase (>3%) indicating an increase in sulfur fugacity (fS_2). This stage has an important role in controlling the mineralization, due to producing open spaces by fractures, joints and brecciation. These assemblages commonly contain quartz, pyrite, arsenian pyrite, chalcopyrite, bornite, chalcocite and covellite together with minor digenite, enargite, galena, native copper, tetrahedrite, tenantite and marcasite. Some of these minerals such as enargite and tetrahedrite are characteristics of epithermal related to subvolcanic or high sulfidation deposits (Hedenquist et al., 2000). Minerals such as enargite, tetrahedrite, tenantite and solid solution of gold in bornite and other Cu-bearing minerals were identified using SEM (Fig. 2). This stage has formed phase III of gold mineralization with grades between 1.5 and 2.5 ppm (Au/Ag greater than 1). The highest mineralization of base metal elements especially copper belongs to this phase. Average Cu grade in this stage is 0.03%.

The fourth stage is the highest phase of gold mineralization accompanied by boiling process. This phase is the continuum of the previous mineralization phase (phase III) and has shaped in form of open space filling and the fractures and joints have controlled the mineralization. The fourth phase presents evidence for decreasing pressure and depositional fluids. Quartz in this phase is little while sulfides are abundant, though the diversity is not as high as for the phase III. Paragenesis mainly comprises sulfide minerals (arsenian pyrite), native gold and electrum in quartz, cristobalite, sericite, barite and fluorite with low contents of base metal sulfides. Most of the gold mineralization (3.5–5 ppm) in the deposit belongs to this phase and correlates with a boiling hydrothermal system. Therefore, mineralization phases of gold in Touzlar deposit are related to hydrothermal breccias and boiling phases (phases III and IV) within which gold is in the form of fine-grained inclusions and solid solution. Scarcely, free gold is found in silicic veinlets.

4. Lithogeochemical interpretation by C–A method

A total of 159 lithogeochemical samples were collected from the deposit, as depicted in Fig. 1, and analyzed by ICP-MS for 42 elements, especially for Au, Ag, As and Cu. Detection limits for Au, Ag, As and Cu are 1 ppb, 10 ppb, 0.5 ppm and 0.2 ppm, respectively. Ordinary PCA, using a correlation matrix of the Au, Ag, As and Cu data, was applied to reduce the number of variables and obtain few uncorrelated variables containing most of the data variance. The correlation coefficients among Au, Ag, As and Cu, range from 0.30 to 0.58 (Table 2).

Elemental distributions were identified by multifractal IDW method in the Touzlar deposit using RockWorks™ 15 software package. For this estimation, variograms of the elements and anisotropic ellipsoid were calculated and generated, as depicted in Fig. 3. Interpolated parameters consist of minimum and maximum searching number of samples and power of IDW which are 3, 10 and 2, respectively. The area was gridded by 5×5 m cells, which were determined based on the geometrical properties of the studied area and grid sampling dimensions (David, 1970). C–A log–log plots were drawn based on reverse relationships between elemental concentrations and their areas, as depicted in Fig. 4. Elemental distributions in the deposit were multifractal based on their log–log plots, as depicted in Fig. 4. Moreover, all elements were grouped in eleven factors, where Au, Ag, Cu and As existed in factor 3 based on PCA method (Table 2).

There are six geochemical populations for Au, five populations for Ag and As and four populations for Cu, as illustrated in Fig. 4. Moreover, there are four mineralization phases for Au within threshold values equal to 0.239, 1.4 and 3.38 ppm where higher than the last threshold value is extreme Au mineralization phase in the deposit, as revealed in Table 3. The populations below 0.239 ppm and between 0.239 and 1.4 ppm are the weak and moderate phase of Au mineralization. In addition, the population between 1.4 and 3.38 ppm has a high mineralization phase of Au in the deposit. It can be considered that the main Au mineralization starts from 1.4 ppm in the Touzlar deposit. According to its log–log plot, Ag mineralization is separated into four phases with 3.16, 15.84 and 52.48 ppm threshold values (Table 3). Weak, moderate, high and extreme mineralization phases are lower than 3.16 ppm, between 3.16 and 15.84 ppm, between 15.84 and 52.48 ppm and higher than 52.48 ppm, respectively. Moreover, As C–A log–log plot presents four phases of mineralization for this element (which are important for Au mineralization) with threshold values equal to 794.32, 7079.46 and 79432 ppm, as shown in Table 3. Weak and moderate As phases are below 794.32 ppm and between 794.32 and 7079.46 ppm, but high and extreme phases have high values of As between 7079.46 and 79432 ppm and higher than 7.9%, respectively. Copper has four enrichment phases in the deposit based on C–A log–log plot of Cu, as depicted in Fig. 4. Their threshold values equaled to 35.48, 158.48 and 398.1 ppm, as presented in Table 3. Extreme enrichment of Cu is higher than 398.1 ppm. Lower than 35.48 ppm is a weak Cu mineralization phase in this area and moderate and high sulfidation occurred between 35.48 and 158.48 ppm and between 158.48 ppm and 398.1 ppm, respectively.

Table 2
Correlation coefficients among Cu, Pb, Zn and Ag and rotated component matrix of factor analysis in the area: loadings in bold represent the selected factors based on threshold of 0.6 in factor 3.

	Au	Ag	As	Cu
Au	1.00			
Ag	0.56	1.00		
As	0.38	0.58	1.00	
Cu	0.50	0.30	0.58	1.00

Rotated component matrix

	Component										
	1	2	3	4	5	6	7	8	9	10	11
Au	−.210	−.143	**.725**	−.147	.012	.005	−.003	−.078	−.102	.260	.147
Cr	.321	.082	.024	.221	.013	−.114	.616	−.014	.083	.348	−.129
Mn	.013	.372	−.058	−.054	.625	.454	.184	−.044	.068	−.019	−.124
Ni	.018	−.006	.007	.067	.916	−.053	.119	−.041	.005	.013	.020
Pb	.013	−.161	.469	.230	−.032	−.033	−.022	.513	−.082	−.284	.337
Sr	.026	−.062	.093	.922	−.009	−.130	−.020	.000	−.023	.064	.085
Ba	.079	−.003	.005	.171	−.030	.205	−.117	.031	.820	.069	−.023
Be	.271	.630	−.286	−.160	.146	.173	.305	.021	.097	.064	.044
Ti	.836	.100	−.268	−.050	−.115	.149	.218	−.074	−.051	.039	−.126
Fe	.331	−.121	.157	.138	.063	−.066	−.016	.193	−.058	.703	.037
Al	.675	.335	−.117	.426	.009	.006	.221	−.068	.117	.186	−.100
La	−.004	.873	−.085	.345	−.044	−.047	−.041	.011	−.037	−.019	.012
Sc	.764	.140	−.147	−.112	.198	.117	.423	−.053	.080	.090	.000
Ca	.226	.014	−.094	−.035	−.018	−.170	.734	−.050	−.157	−.220	.056
Li	−.153	−.038	.214	.786	−.019	−.203	.027	−.041	.228	.043	−.017
P	.076	.181	−.158	.778	−.074	.142	−.062	.034	−.238	.092	−.168
V	.788	.038	−.203	.285	.144	−.067	.092	.060	.073	.203	−.018
Mg	.346	.158	−.169	−.263	.252	.256	.631	−.045	−.200	−.090	−.155
K	.378	.302	−.234	−.356	−.125	.641	.027	−.130	.061	.037	.118
Na	.113	.569	−.099	−.289	.033	.213	.182	−.203	−.045	.050	−.216
S	−.099	−.203	.066	.207	−.226	.159	−.002	−.070	−.749	.196	.010
Zr	.743	.144	−.109	−.194	.096	.129	.098	−.127	.123	−.128	−.004
Ag	−.132	−.034	**.872**	−.088	.047	.163	−.023	.021	−.023	.071	.100
As	−.086	−.064	**.661**	−.010	−.052	−.004	−.015	.627	.015	−.181	.080
Bi	−.287	−.215	.313	.191	.088	−.174	−.174	−.069	−.104	.518	.345
Co	.146	.080	.026	−.018	.851	−.132	−.156	−.068	−.016	−.027	.033
Cu	−.101	−.008	**.813**	−.039	.109	−.136	−.043	.182	.086	.219	−.073
Mo	−.326	−.143	.481	.356	−.187	.100	.008	.082	.141	−.263	−.036
Sb	−.265	−.206	.645	.159	.048	−.043	−.148	.197	.168	.192	.075
Zn	.022	.236	−.136	−.177	.606	.147	.397	.274	.173	.148	.086
Sn	−.212	−.055	.706	.090	−.046	−.150	−.174	.241	−.030	−.034	.097
W	.420	.323	.152	−.120	−.048	.203	−.244	−.003	.302	.064	.342
Cs	.460	.143	−.297	−.401	−.350	.276	.158	−.017	−.195	−.016	.096
Nb	.724	.390	−.313	−.218	−.080	.127	−.016	−.039	−.051	−.040	−.152
U	.338	.590	.086	−.045	.378	−.297	−.213	.106	.130	−.094	.050
Te	−.093	−.110	.860	.057	−.062	.029	.005	−.017	−.035	.091	−.070
Cd	−.139	.016	−.162	−.034	.682	.025	.007	.477	.092	.155	.029
Rb	.344	.268	−.308	−.454	−.175	.568	.054	−.077	.018	−.039	.127
Th	.375	.835	−.134	−.097	.019	.042	−.001	−.088	.102	−.112	−.020
Y	.220	.732	−.106	−.276	.347	.095	.207	.026	.054	−.083	−.037
Ce	.024	.932	−.149	.144	.034	−.006	.001	.002	.037	−.042	.011
Tl	.081	−.083	.089	−.008	.034	.784	−.125	−.051	.055	−.106	.106

Based on geological study and its correlation with results obtained from C–A model, first population for Au in C–A log–log plot (<0.239 ppm) correlated with pre-mineralization and phase I that cannot be separated due to Au low grades. Moreover, there is a topic correlation between low grade mineralization resulted from geological model and weak Au mineralization derived via C–A model. Multifractal behavior in C–A log–log plots of Ag and As and their main mineralization are correlated with pre-mineralization and phase I obtained by geological investigations. However, the geological phases are correlated with the forth population of Ag (15.84–52.48 ppm) and fifth population or extreme As mineralization (>7.9%) which are distinguished by arsenian minerals and base metal sulfides especially galena. Second population of Cu (35.48–158.438 ppm) is associated with the geological phases because there is low sulfidation in these phases.

Second and third populations of Au mineralization resulted from C–A model (moderate mineralization) with Au values between 0.239 and 1.4 ppm have a direct relationship with phase II mineralization for the geological model. Silver shows extreme mineralization in this phase because of its increase in As minerals and galena. Mineralization is weak for As and Cu based on C–A model because sulfides were used for pyrite and galena mineralization.

High mineralization of Au obtained by C–A model has a strong correlation with phase III resulted from geological model (brecciation) which has Au values between 1.4 and 3.28 ppm due to increase in effective porosity through brecciation and influx of high sulfidation hydrothermal fluids. Copper grade is highest in this phase and is correlated with extreme mineralization based on C–A model (>398.1 ppm). Increase in Au and Cu grades is based on chalcopyrite and arsenopyrite occurrences because high

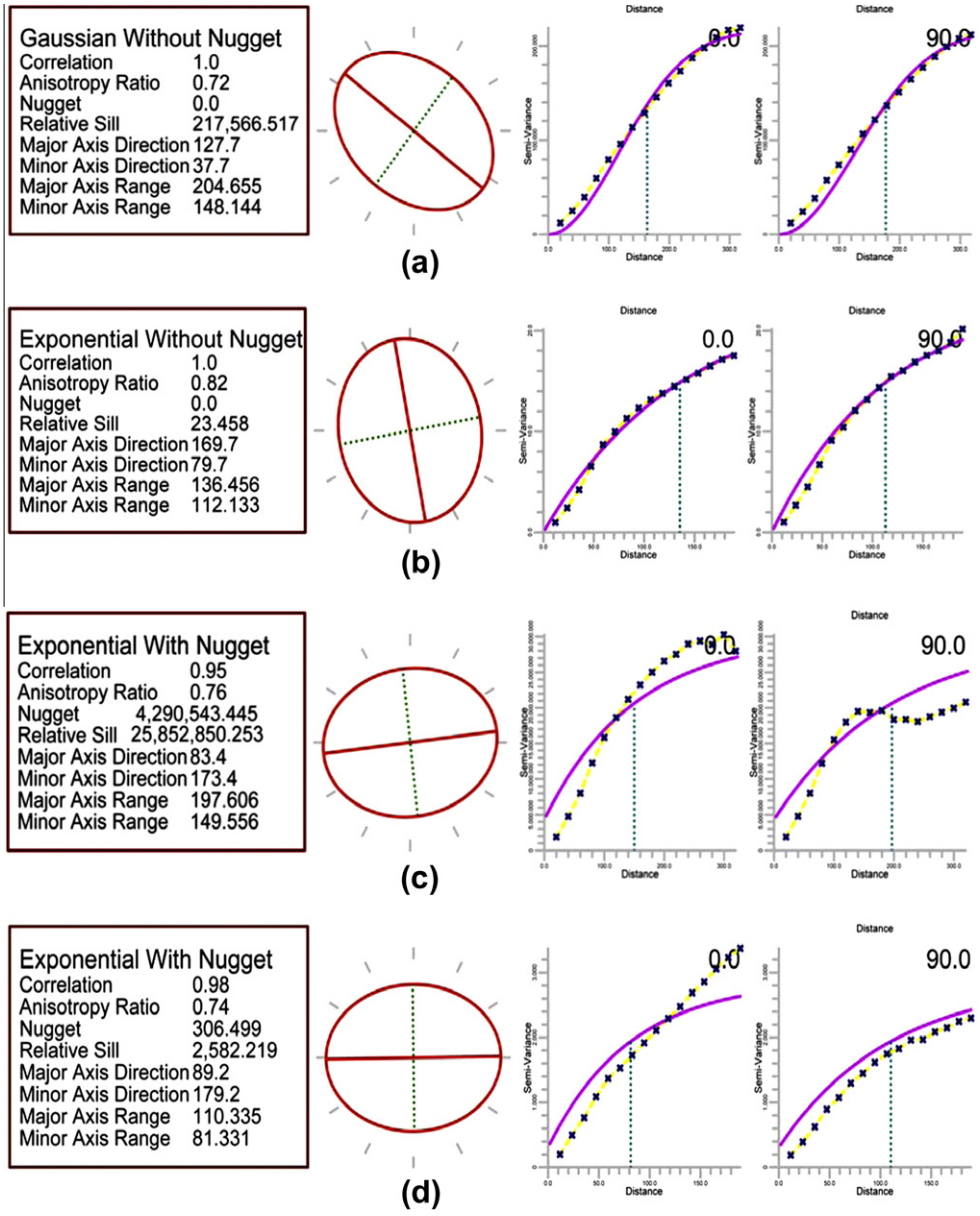

Fig. 3. Experimental variograms of Au (a), Ag (b), As (c) and Cu (d) for lithogeochemical data from Touzlar deposit.

amounts of Au grains existed in the minerals. Silver values are lower than the previous phases based on decreasing galena content.

Extreme Au mineralization based on C–A model is correlated with the fourth phase of the geological model, which is boiling processes. Main sulfidation filled fractures and open spaces specifically in form of arsenopyrite and pyrite. High mineralization of As derived from C–A model exists in the phase based on increasing arsenopyrite. However, Cu mineralization is third level (158.48–398.1 ppm) due to C–A model because Cu sulfides occurred in the phase. Weak mineralization of Ag is associated with the phase because no galena is reported.

Elemental maps generated by RockWorks™ 15 are shown in Fig. 5. Gold extreme anomalous parts (higher than 4.4 ppm) are located in NE portion of the central part of the deposit. Gold high intensity phases (between 1.4 and 3.38 ppm) occurred in NE, SW and central parts of the deposit. Gold mineralization (higher than 1.4 ppm) has a NE–SW trend in the deposit, as illustrated in Fig. 5. Silver anomalies are divided into two separate parts, as presented in Fig. 3. Extreme Ag mineralization phases above 52.48 ppm have been located in southern part of the area, but the northern part contains lower grade of Ag anomalies. The northern part correlates with moderate and high Au mineralization phases based on C–A method. High Ag mineralization phase between 15.84 and 52.48 ppm is located in southern and northern parts of the Touzlar deposit, as shown in Fig. 5. Arsenic anomaly distribution correlates with Au anomalous parts in the deposit, as illustrated in Fig. 5. Extreme As phase occurring in NE part of the deposit correlates with the Au extreme phase. High and moderate phases of As correlate with the Au mineralization phase in central part of the deposit. Copper concentration distributions associate with Au major phase in central part of the deposit. On the other hand, Cu values higher than 398.1 ppm occurred in central part of the area and correlate with high grade phase of Au (over 3.38 ppm). The main Cu mineralization has a trend from central to SW part of the deposit, as shown in Fig. 5.

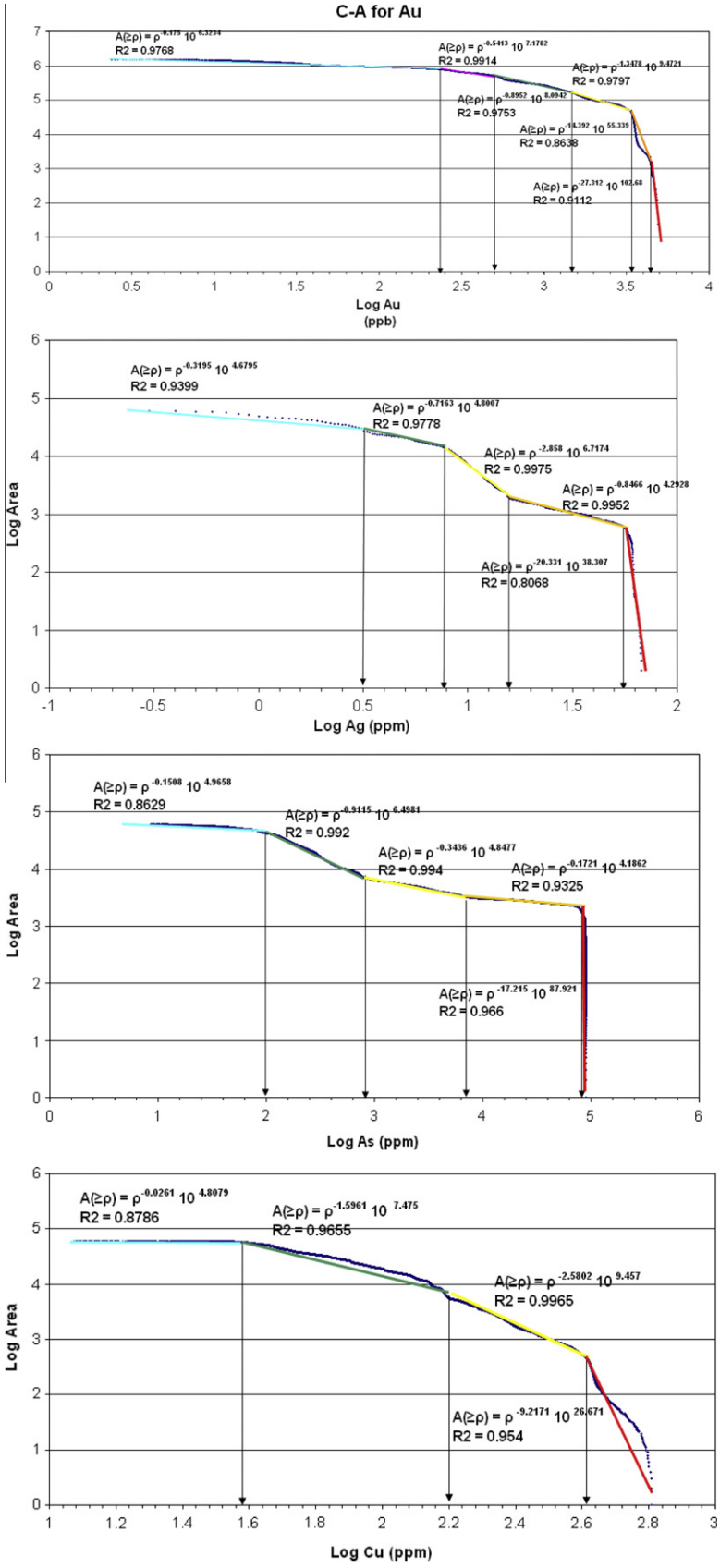

Fig. 4. C–A log–log plots for Au, Ag, As and Cu in Touzlar deposit.

Table 3
Element thresholds from C–A method.

Anomaly intensive (ppm)	Moderate	High	Extreme
Au	0.239	1.4	3.38
Ag	3.16	15.8	52.5
As	794	7080	79400
Cu	35.5	158	398

5. Comparison with geological and mineralization characteristics

Elemental geochemical phase ranges from C–A method, are compared and correlated with specific geological characteristics of the deposit including considering natural silicic veins and faults. Gold, silver, arsenic and copper distributions in the Touzlar deposit, and the faults map are shown in Fig. 6. The anomalous parts, specifically extreme and high grades, clearly depict the main identified faults especially in central and NE parts of the deposit. These parts correlate with existing structural settings and controls as illustrated in Fig. 6.

Gold, silver and arsenic anomalies show that the faults intersect the anomalies located near those structures and depict a positive relationship between elemental anomalies and faults (Fig. 6). Extreme and high grades elemental anomalies occurred inside and within the fault zones or located on the fault intersection areas, as illustrated in Fig. 6.

Based on the geological studies and evidences in the Touzlar deposit, Au mineralization resulted from C–A method is correlated with faults, silicic veins and mineralization phases. The Au extreme phase with Au values higher than 3.38 ppm, relates to fractures and open spaces which have been formed after silicic veins, as indicated in phase IV (main sulfidation) with no association with silicic veins, as illustrated in Table 4. According to geological characteristics, high-grade mineralization correlates with fractures, hydrothermal breccias and not so much with silicic veins (phase III) in the area, that located around extreme Au mineralization from C–A method and related with C–A high Au mineralization stage, as presented in Table 4. The C–A moderate Au mineralization phase correlates with phase II and their related faults (silicic veins). The weak Au phase from C–A method (lower than 239 ppb) has a

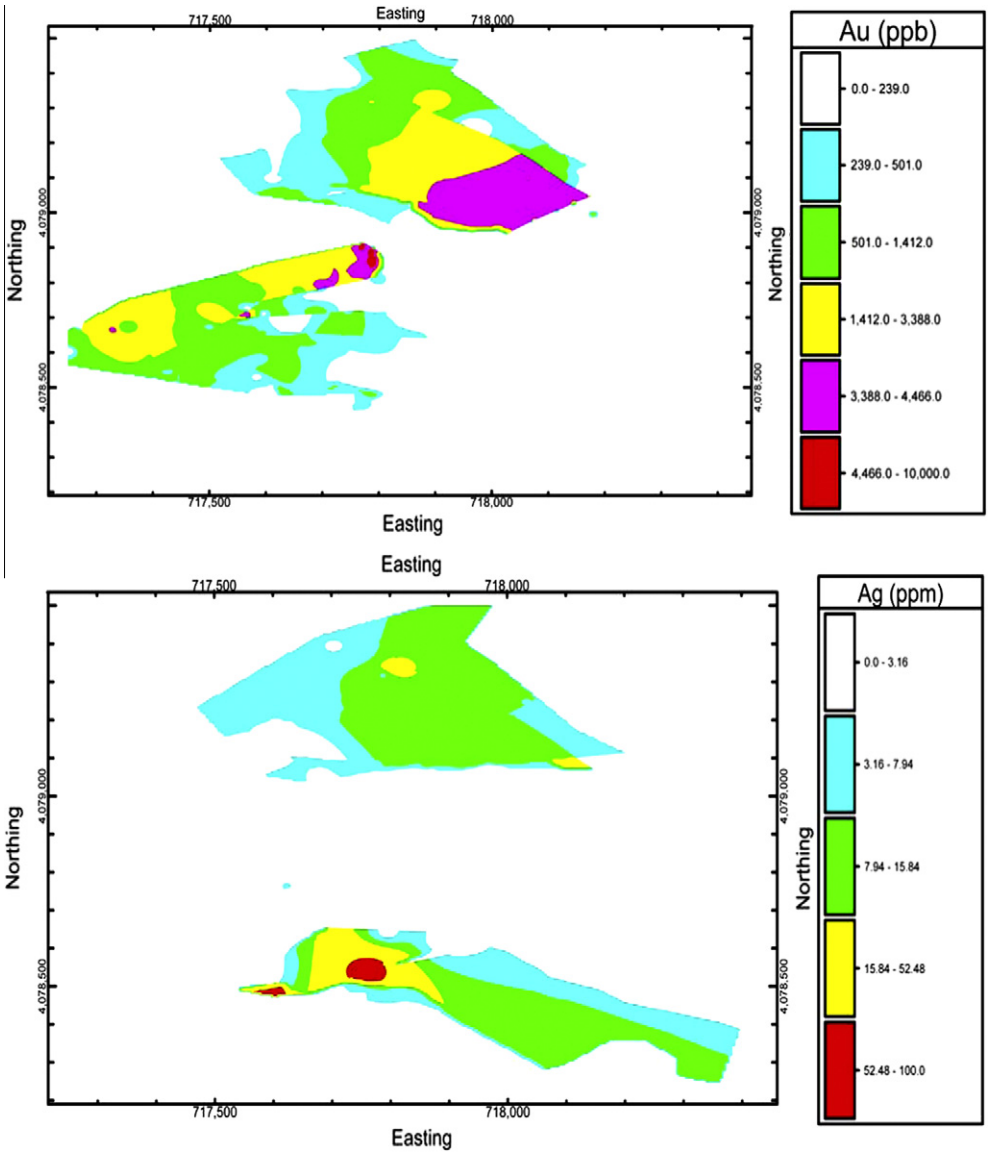

Fig. 5. Au, Ag, As and Cu geochemical population distribution maps based on C–A method.

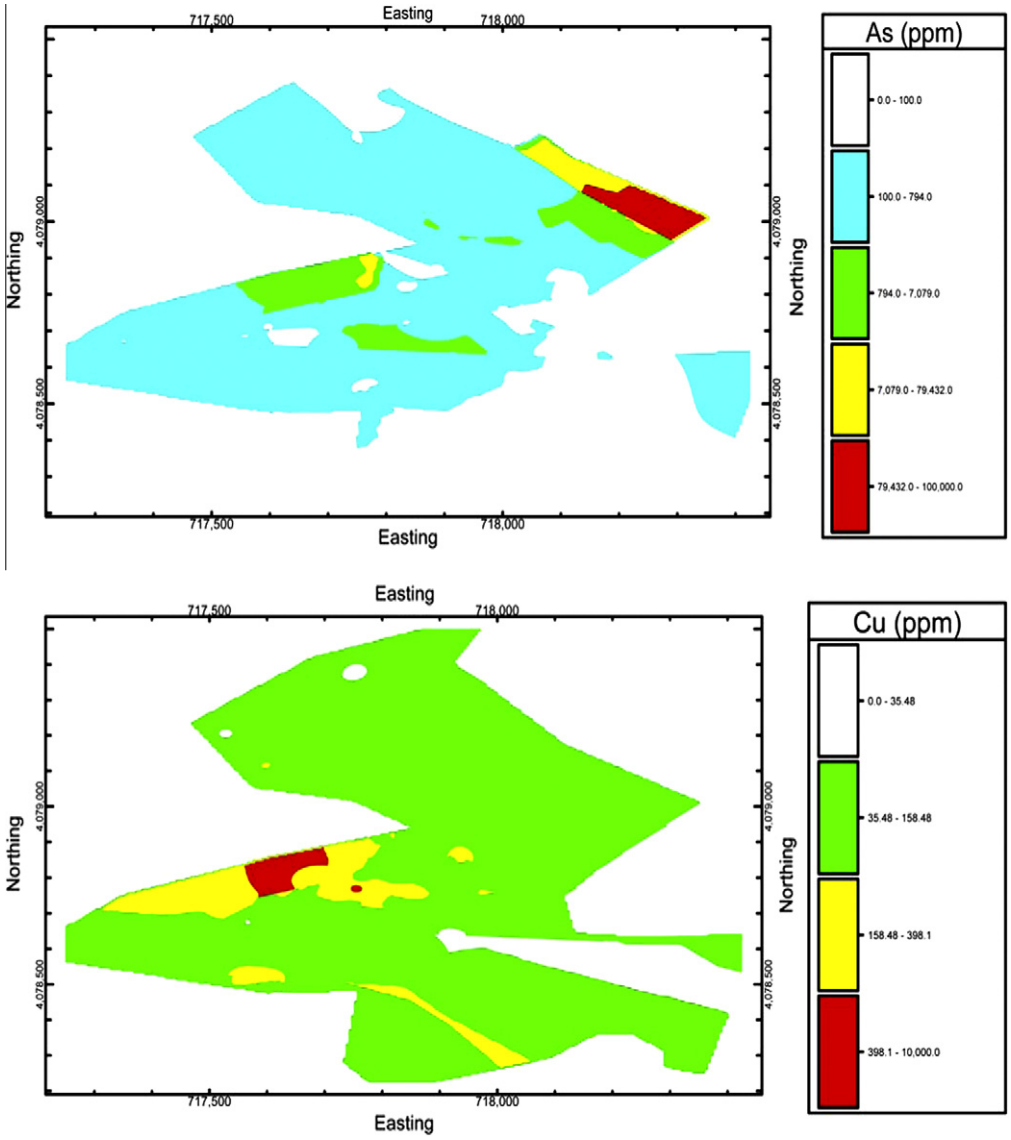

Fig. 5. (*continued*)

strong correlation with the silicified zone in phase I, as depicted in Table 4.

Pre-mineralization and phase I have Au values lower than 0.239 ppm shown by the first segment of Au C–A log–log plot consisting of background for volcanic host rocks (10–20 ppb) and the first hydrothermal mineralization phase. Phase II includes Au values between 0.239 and 1.4 ppm, which is indicated by the second and third segments in the log–log plot. Both segments existing in phase II illustrate sub-phases of mineralization with their separation being difficult through mineralographical study. The fourth segment indicates phase III, with Au values between 1.4 and 3.38 ppm. The final phase of gold mineralization consists of boiling and weathering processes shown in the fifth and final segments of the Au C–A plot. Weathering processes resulted in an increase in Au values in the final phase with secondary enrichment.

Silver anomalies in the Touzlar deposit have a good correlation with faults and silicic veins as depicted in Fig. 6. Extreme phase of Ag resulted from C–A method and higher than 52.48 ppm, is correlated with silicic veins, as shown in phase II (Table 4). C–A high mineralization phase of Ag, associated with phase I has been nominated silicified zone in the deposit. Moderate Ag phase from C–A model is related to phase III including hydrothermal breccias and sulfur content higher than 10% and weak Ag mineralization phase resulted from C–A method, correlates with phase IV (main sulfidation).

Arsenic anomalies have relationship with faults and silicic veins in the Touzlar deposit, as presented in Fig. 6. In addition, extreme phase (higher than 7.9% based on C–A method) is correlated with silicified zone equal to phase I, as depicted in Table 4. High As phase between 0.7% and 7.9% resulted from C–A model, is associated with phase IV, named as main sulfidation phase based on geological studies. The C–A moderate phase is correlated with hydrothermal breccias and fractures named as phase III. Weak mineralization phase of As based on C–A method relates with the silicic veins. Geological studies and evidences reveal that silicic veins are associated with phase II, as shown in Table 3.

Distribution of Cu anomalies as a minor element in the Touzlar deposit relates with faults and silicic veins, as shown in Fig. 6, but based on obvious geological evidences it has a strong correlation with breccias. The extreme Cu mineralization phase from C–A, more than 398.1 ppm, relates to phase III, resulted from hydrothermal breccias and their fractures, as depicted in Table 2. Also, high Cu concentration phase between 158.48 and 398.1 ppm resulted from C–A method is correlated with phase IV, including main

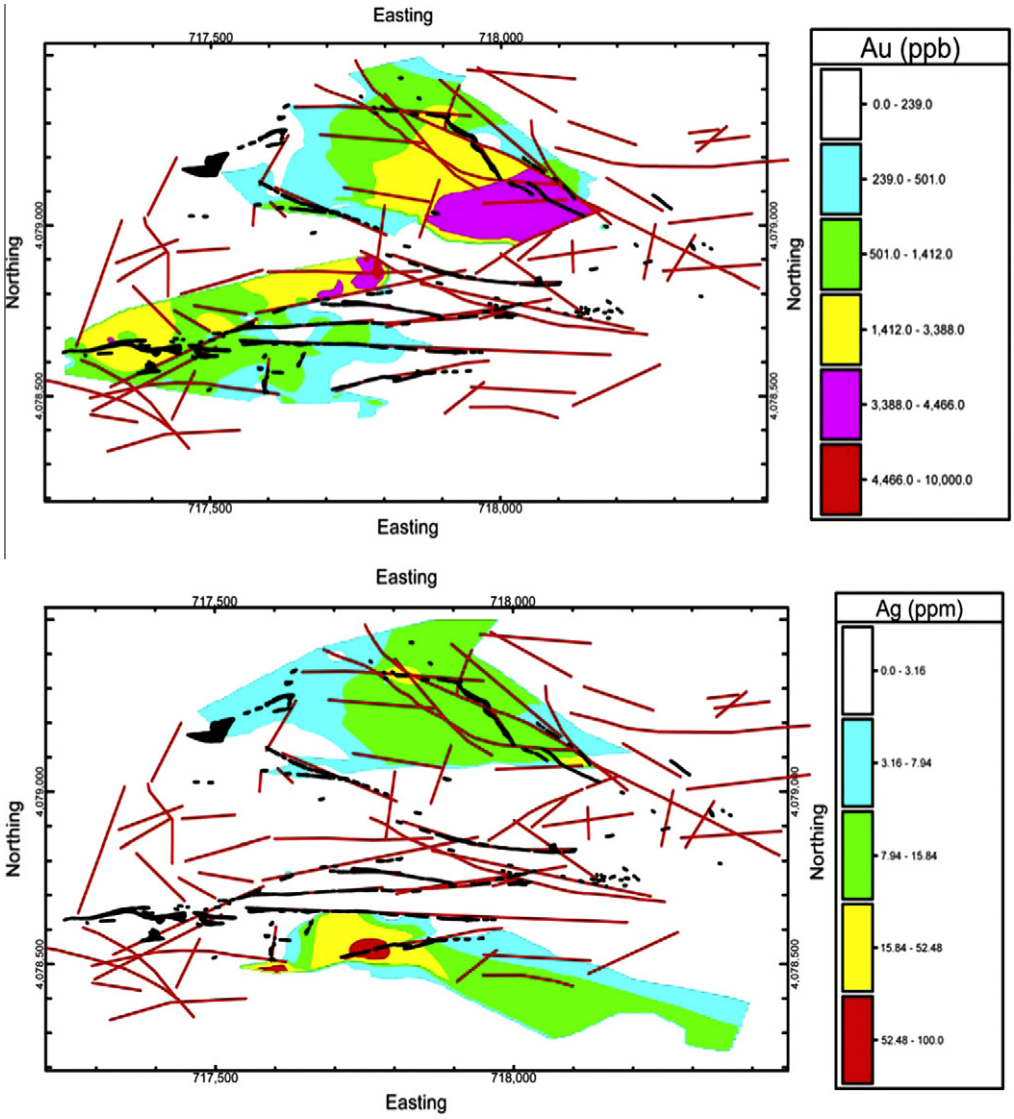

Fig. 6. Relationship between Au, Ag, As and Cu distribution and silicic alteration (black lines) and faults (red lines) in Touzlar deposit. (For interpretation of the references to color in this figure legend, the reader is referred to the web version of this article.)

sulfidation and high amounts of sulfide minerals. Phase I of geological characteristics, named as silicified zone, is associated with C–A moderate Cu mineralization phase. Weak Cu phase from C–A model is related to silicic veins in phase II.

6. Conclusions

Study of Touzlar Au–Ag (Cu) epithermal deposit based on C–A multifractal modeling reveals that there are four main phases of mineralization for Au, Ag, As and Cu. Moreover, the number of mineralization phases resulted from multifractal modeling is equal to the number of mineralization phases depicted from geological study including field geology, petrographical and mineralographical, EPMA and XRD studies.

The weak, moderate, high and extreme mineralization phases, obtained from the resulting C–A method, have high spatial correlation with geological studies.

Pre-mineralization and phase I including silicified zone with low values of sulfide minerals correlate with weak Au mineralization phase (lower than 239 ppb), high Ag phase (15.84 and 52.48 ppm), extreme mineralization stage of As (higher than 7.9%) and moderate phase of Cu mineralization (35.45 and 158.48 ppm). In this phase, mineralization is distributed in high volume of silicic zone with an important role in decreasing Au mineralization grade. Phase II including silicic veins and veinlets and related faults correlates with Au moderate phase between 239 ppb and 1.4 ppm, Ag extreme mineralization (above 52.48 ppm) and As and Cu weak phases (lower than 794.32 ppm and 35.48 ppm, respectively). Phase III represented by hydrothermal breccias and their fractures within sulfur content over 10%, associates with high Au phase between 1.4 and 3.38 ppm, moderate phase for Ag between 3.16 and 15.84 ppm and As between 794.32 and 7079.46 ppm and extreme phase of Cu mineralization higher than 398.1 ppm. Additionally, phase III distinguished by base metals, mainly Cu, correlates with the sulfidation zone (higher than 3%). There is main mineralization of Au and Cu because of high values of brecciation and sulfidation, especially in form of chalcopyrite. Phase IV, distinguished by very high sulfidation and sulfide minerals has a strong relationship with Au extreme (above 3.38 ppm), Ag weak phase (below 3.16 ppm), As and Cu high mineralization phase between 0.7% and 7.9% and between 158.48 and

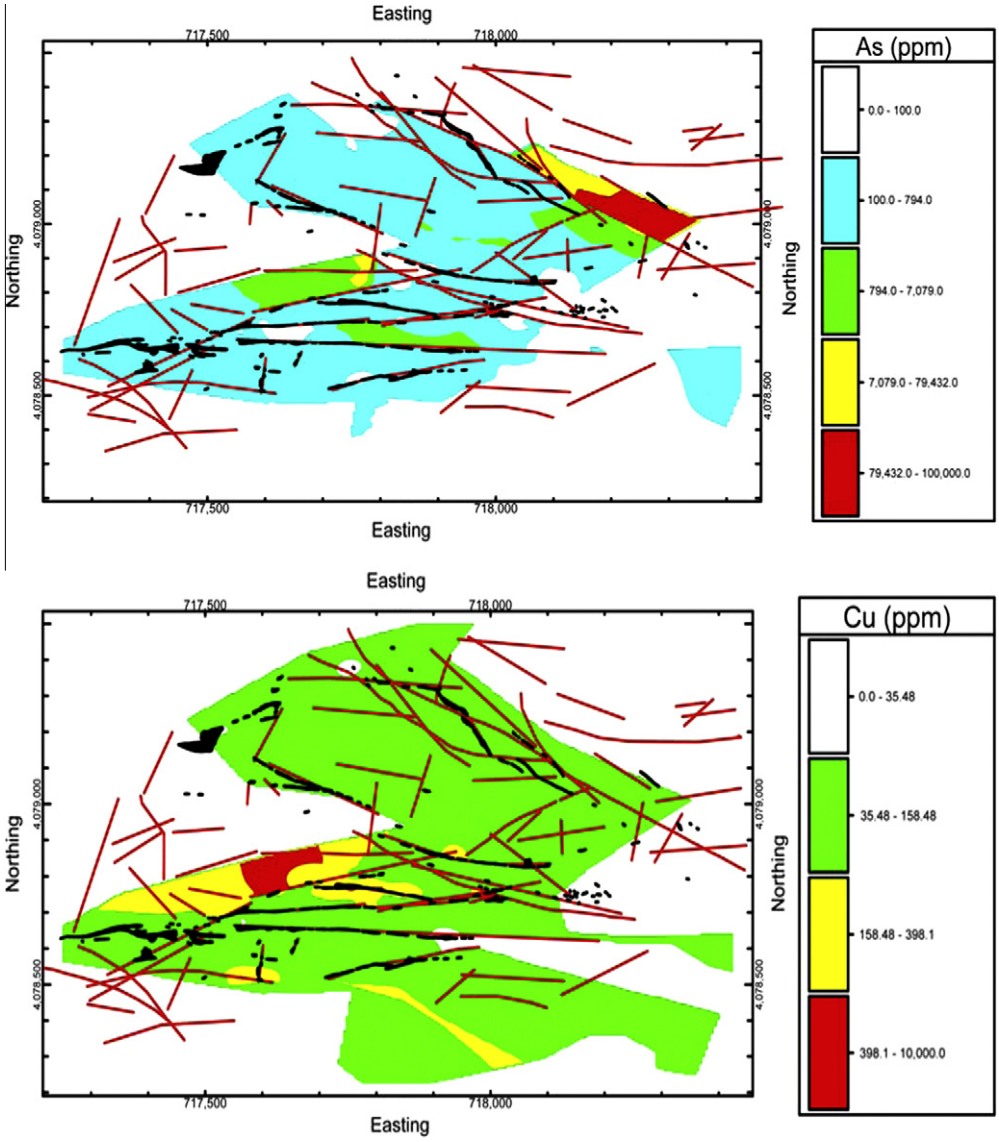

Fig. 6. (*continued*)

Table 4
Correlation between geological mineralization phases and phases resulted from C–A method.

Geological mineralization phase	Phase I (silicified zone)	Phase II (silicic veins)	Phase III (hydrothermal breccia)	Phase IV (main sulfidation)
Au phase	Weak	Moderate	High	Extreme
Ag phase	High	Extreme	Moderate	Weak
As phase	Extreme	Weak	Moderate	High
Cu phase	Moderate	Weak	Extreme	High

398.1 ppm, respectively. Extreme Au mineralization based on C–A model has a relationship with boiling processes and separation of sulfide and silica.

Results from multifractal modeling in comparison with geological characteristics reveal that Au and Ag have two different mineralization trends with converse relationship. The extreme and high phases of Ag have a minor relationship with Au in southern part of the deposit. In the northern part, mineralization sequence is complex because many phases of Au and Ag occur in different stages. Extreme phase of As in the area belongs to the weak stage of Ag and the moderate phase of Au. Most of the Au phases correlate with moderate to high phases of As. Furthermore, based on C–A method, Cu extreme and high phases exist within hydrothermal breccias and main sulfidation phase. In addition, extreme Cu phase correlates with high amounts of sulfide minerals, such as chalcopyrite and bornite. Additionally, mineralographical studies, silicification, silicic veins and veinlets and fault setting confirm the accuracy of the results obtained from C–A method. Extreme and high phases of these elements correlate directly with silicification, sulfidation and hydrothermal processes.

Delineation of mineralization phases based on the C–A method and multifractal nature of C–A log–log plots could be of essential help to geoscientists for interpreting the phases in which an element is enriched in a deposit. This method can help us better understand and separate mineralizations in epithermal deposits based on lithogeochemical data.

Acknowledgements

The present study is a part of first author's PhD thesis at Tarbiat Modares University, Tehran, Iran. Field studies and laboratory costs were partly funded by the Tarbiat Modares University Research Grant Council. The authors wish to thankfully acknowledge contributions from Dr M. Momenzadeh, Mr M. Hosseini and Ms L. Berahmand of Zaryaban Consultant Company, Tehran, Iran for authorizing the use of geochemical data set of Touzlar area. Ms N. Hassani and the editors and reviewers of Applied Geochemistry are also thanked for editing the text and their constructive remarks.

References

Aftabi, A., Atapour, H., 2000. Regional aspects of shoshonitic volcanism in Iran. Episodes 23, 119–125.

Afzal, P., Khakzad, A., Moarefvand, P., Rashidnejad Omran, N., Esfandiari, B., Fadakar Alghalandis, Y., 2010. Geochemical anomaly separation by multifractal modeling in Kahang (Gor Gor) porphyry system, Central Iran. J. Geochem. Explor. 104, 34–46.

Afzal, P., Khakzad, A., Moarefvand, P., Rashidnejad Omran, N., Fadakar Alghalandis, Y., 2011. Delineation of mineralization zones in porphyry Cu deposits by fractal concentration–volume modeling. J. Geochem. Explor. 108, 220–232.

Agard, P., Omrani, J., Jolivet, L., Mouthereau, F., 2005. Convergence history across Zagros (Iran): constraints from collisional and earlier deformation. Int. J. Earth Sci. 94, 401–419.

Agterberg, F.P., Cheng, Q., Wright, D.F., 1993. Fractal modeling of mineral deposits. In: Elbrond, J., Tang, X. (Eds.), 24th APCOM Symposium Proceeding, Montreal, Canada, pp. 43–53.

Agterberg, F.P., Cheng, Q., Brown, A., Good, D., 1996. Multifractal modeling of fractures in the Lac du Bonnet batholith, Manitoba. Comput. Geosci. 22 (5), 497–507.

Alavi, M., 1994. Tectonic of the Zagros orogenic belt of Iran: new data and interpretations. Tectonophysics 229, 211–238.

Alavi, M., 2004. Regional stratigraphy of the Zagros fold-thrust belt of Iran and its proforeland evolution. Am. J. Sci. 304, 1–20.

Alavi, M., Hajian, J., Amidi, M., Bolourchi, H., 1982. Geology of the Takab-Saein-Qal'eh. Geol Surv Iran, Rpt 50, 99p.

Ali, Kh., Cheng, Q., Zhijun, C., 2007. Multifractal power spectrum and singularity analysis for modeling stream sediment geochemical distribution patterns to identify anomalies related to gold mineralization in Yunnan Province, South China. Geochem. Explor. Environ. Anal. 7 (4), 293–301.

Allen, M.B., Blanc, E.J.P., Walker, R., Jackson, J., Talebian, M., Ghassemi, M.R., 2006. Contrasting Styles of Convergence in the Arabia–Eurasia Collision: Why Escape Tectonics Does Not Occur in Iran. Geological Society of America, Special Paper 409.

Amidi, S.M., Emami, M.H., Michel, R., 1984. Alkaline character of Eocene volcanism in the middle part of central Iran and its geodynamic situation. Geol. Rundsch. 73, 917–932.

Asadi Haroni, H., Vocken, J.H.L., Kanel, R.A., Hale, M., 2000. Petrography, mineralogy and geochemistry of the Zarshuran Carlin-like gold deposit, northwest Iran. Miner. Deposita 35, 656–671.

Berberian, M., King, G.C.P., 1981. Towards a paleogeography and tectonic evolution of Iran. Can. J. Earth Sci. 18, 210–265.

Berberian, F., Muir, I.D., Pankhurst, R.J., Berberian, M., 1982. Late Cretaceous and early Miocene Andean-type plutonic activity in northern Makran and Central Iran. J. Geol. Soc. London 139, 605–614.

Bolviken, B., Stokke, P.R., Feder, J., Jossang, T., 1992. The fractal nature of geochemical landscapes. J. Geochem. Explor. 43, 91–109.

Boyce, A.J., Fulgnati, P., Sbrana, A., Fallick, A.E., 2007. Fluids in early stage hydrothermal alteration of high-sulfidation epithermal systems: A view from the volcano active hydrothermal system (Aeolian Island, Italy). J. Volcanol. Geoth. Res. 166, 76–90.

Carranza, E.J.M., 2008. Geochemical anomaly and mineral prospectivity mapping in GIS. Handbook of Exploration and Environmental Geochemistry, vol. 11. Elsevier, Amsterdam.

Carranza, E.J.M., 2009. Controls on mineral deposit occurrence inferred from analysis of their spatial pattern and spatial association with geological features. Ore Geol. Rev. 35 (3–4), 383–400.

Carranza, E.J.M., Sadeghi, M., 2010. Predictive mapping of prospectively and quantitative estimation of undiscovered VMS deposits in Skellefte district (Sweden). Ore Geol. Rev. 38, 219–241.

Cheng, Q., 1999. Spatial and scaling modelling for geochemical anomaly separation. J. Geochem. Explor. 65 (3), 175–194.

Cheng, Q., 2007. Mapping singularities with stream sediment geochemical data for prediction of undiscovered mineral deposits in Gejiu, Yunnan Province, China. Ore Geol. Rev. 32, 314–324.

Cheng, Q., Agterberg, F.P., 1996. Multifractal modeling and spatial statistics. Math. Geol. 28 (1), 1–16.

Cheng, Q., Agterberg, F.P., 2009. Singularity analysis of ore-mineral and toxic trace elements in stream sediments. Comput. Geosci. 35 (2), 234–244.

Cheng, Q., Agterberg, F.P., Ballantyne, S.B., 1994. The separartion of geochemical anomalies from background by fractal methods. J. Geochem. Explor. 51, 109–130.

Chouinard, A., Williams-Jones, A.E., Leonardson, R.W., Hodgson, C.J., 2005. Geology and genesis of the multistage high sulfidation epithermal Pascua Au–Ag-Cu deposit, Chile and Argentina. Econ. Geol. 100, 463–490.

Cooke, D.R., Simmons, S.F., 2000. Characteristics and genesis of epithermal gold deposits: Society of Economic Geologists. Reviews in Economic Geology 13, 221–244.

Craig, G.R., Vaughan, D., 1994. Ore Microscopy and Ore Petrography. John Wiley and Sons, 434 p.

Daliran, F., 2007. The carbonate rock-hosted epithermal gold deposit of Agdarreh Takab geothermal field, NW Iran-hydrothermal alteration and mineralization. Miner. Deposita 43 (4), 383–404.

Daliran, F., Hofstra, A.H., Walther, J., Stüben, D., 2002. Agdarreh and Zarshouran SRHDG deposits, Takab region, NW-Iran. In: GSA Annual Meeting 2002, Abstr with Prog, Session 63–8.

David, M., 1970. Geostatistical Ore Reserve Estimation. Elsevier, Amsterdam, 283 p.

Davis, J.C., 2002. Statistics and Data Analysis in Geology, 3rd ed. John Wiley & Sons Inc, New York.

Emami, M.H., 2000. Magmatism in Iran. Geological Survey of Iran, 620 p.

Evertz, C.J.G., Mandelbrot, B.B., 1992. Multifractal measures (appendix B). In: Peitgen, H.-O., Jurgens, H., Saupe, D. (Eds.), Chaos and Fractals. Springer, New York.

Faure, K., Matsuhisa, Y., Metsugi, H., Mizota, C., Hayashi, S., 2002. The Hishikari Au–Ag epithermal deposit, Japan: oxygen and hydrogen isotope evidence in determining the source of paleohydrothermal fluids. Econ. Geol. 97, 481–498.

Ghasemi, A., Talbot, C.J., 2006. A new tectonic scenario for the Sanandaj–Sirjan Zone (Iran). J. Asian Earth Sci. 26, 683–693.

Glennie, K.W., 2000. Cretaceous Tectonic Evolution of Arabia's Eastern Plate Margin: A Tale of Two Oceans. Society for Sedimentary Geology (SEPM) Special Publication, vol. 69, pp. 9–20.

Goldfarb, R.J., Hart, C., Davis, G., Groves, D., 2007. East Asian gold: Deciphering the anomaly of Phanerozoic gold in Precambrian cratons. Econ. Geol. 102 (3), 341–347.

Goncalves, M.A., Vairinho, M., Oliveira, V., 1998. Study of geochemical anomalies in Mombeja area using a multifractal methodology and geostatistics. In: Buccianti, A., Nardi, G., Potenza, R. (Eds.), IV IAMG'98. De Frede, Ischia Island, Italy, pp. 590–595.

Goncalves, M.A., Mateus, A., Oliveira, V., 2001. Geochemical anomaly separation by multifractal modeling. J. Geochem. Explor. 72, 91–114.

Groves, D.I., Bierlein, F.P., 2007. Geodynamic settings of mineral deposit systems. Journal of the Geological Society 2007 (164), 19–30.

Groves, D.I., Vielreiche, R.M., Goldfarb, R.J., Condie, K.C., 2005. Controls on the heterogeneous distribution of mineral deposits through time, Mineral Deposits and Earth Evolution. Geological Society, London, Special Publications 248, 71–101.

Halsey, T.C., Jensen, M.H., Kadanoff, L.P., Procaccia, I., Shraiman, B.I., 1986. Fractal measures and their singularities: the characterization of strange sets. Phys. Rev. A 33 (2), 1141–1151.

Hassanzadeh, J., 1993. Metallogenic and Tectonomagmatic Events in the SE Sector of the Cenozoic Active Continental Margin of Central Iran (Shahr e Babak area, Kerman Province) [Ph.D. Thesis]: Los Angeles, University of California, 204 p.

Hassanzadeh, J., Stockli, D.F., Horton, B.K., Axen, G.J., Stockli, L.D., Grove, M., Schmitt, A.K., Walker, J.D., 2008. U–Pb zircon geochronology of late Neoproterozoic–Early Cambrian granitoids in Iran: implications for paleogeography, magmatism, and exhumation history of Iranian basement. Tectonophysics 8, 71–96.

Hedenquist, J.W., Arribas, R.A., Gonzalez-Urien, E., 2000. Exploration for epithermal gold deposits. In: Hagemann, S.G. (Ed.), Gold in 2000. Reviews in Economic Geology, vol. 13, pp. 245–277.

Hoefs, J., 2009. Stable Isotope Geochemistry. Springer-Verlag, Berlin, Heidelberg,, 293 p.

Hudson, D.M., 2003. Epithermal alteration and mineralization in the Comstock district, Nevada. Econ. Geol. 98, 367–385.

Jensen, E.P., Barton, M.D., 2000. Gold deposits related to alkaline magmatism. Reviews in Economic Geology 13, 210–314.

Kazmin, V.G., Sbortshikov, I.M., Ricou, L.-E., Zonenshain, L.P., Boulin, J., Knipper, A.L., 1986. Volcanic belts as markers of the Mesozoic-Cenozoic active margin of Eurasia. Tectonophysics 123, 123–152.

Li, C., Ma, T., Shi, J., 2003. Application of a fractal method relating concentrations and distances for separation of geochemical anomalies from background. J. Geochem. Explor. 77, 167–175.

Lima, A., De Vivo, B., Cicchella, D., Cortini, M., Albanese, S., 2003. Multifractal IDW interpolation and fractal filtering method in environmental studies: an application on regional stream sediments of (Italy), Campania region. Appl. Geochem. 18, 1853–1865.

Mandelbrot, B.B., 1983. The Fractal Geometry of Nature. W. H Freeman, San Francisco, 468 p.

Mehrabi, B., Yardley, B.W.D., Cann, J.R., 1999. Sediment-hosted disseminated gold mineralization at Zarshuran, north-west Iran. Miner. Deposita 34, 673–696.

Meng, X., Zhao, P., 1991. Fractal method for statistical analysis of geological data. Chinese Journal of Geosciences 2, 207–211.

Pirajno, F., 1992. Hydrothermal Mineral Deposits—Principles and Fundamental Concepts for the Exploration Geologist. Springer-Verlag, Berlin, 709 p.
Pirajno, F., 2009. Hydrothermal Processes and Mineral Systems. Springer, The University of Western Australia,, Perth, 1273 p.
Pirajno, F., Bagas, L., 2002. Gold and silver metallogeny of the South China Fold Belt: a consequence of multiple mineralizing events? Ore Geol. Rev. 20, 109–126.
Rabiei, A., Kousari, S., Hosseini, M., 2006. Alteration, mineralization and genesis of Touzlar gold deposit. In: Proceedings of the 24th Symposium on Geosciences, Geological Survey of Iran, Tehran, Iran, 27 February–1 March 2006 (in Persian with English abstract, CD-ROM).
Richards, J.P., 1995. Alkalic-type epithermal gold deposits. Mineralogical Association of Canada Short Course Handbook 23, 367–400.
Richards, J., Wilkinson, D., Ulrich, T., 2006. Geology of the Sari Gunay epithermal gold deposit, northwest Iran. Econ. Geol. 101 (8), 1455–1496.
Robb, L., 2005. Introduction to Ore Forming Processes. Blackwell Publishing, 373 p.
Sahandi, M.R., Delavar, S.T., Sadeghi, M., Jafari, A., Moosavi, A., 2005. Geological Map of Iran (1:1,000,000). Geological Survey of Iran. <http://www.ngdir.ir>.
San Shen, J.J., Yang, H.J., 2004. Sources and genesis of the Chinkuashih Au–Cu deposits in northern Taiwan: constraints from Os and Sr isotopic compositions of sulfides. Earth Planet. Sci. Lett. 222, 71–83.
Shafiei, B., Haschke, M., Shahabpour, J., 2009. Recycling of orogenic arc crust triggers porphyry Cu mineralization in Kerman Cenozoic arc rocks, southeastern Iran. Miner. Deposita 44, 265–283.
Shahabpour, J., 2005. Tectonic evolution of the orogenic belt in the region located between Kerman and Neyriz. J. Asian Earth Sci. 24, 405–417.
Shen, W., Zhao, P., 2002. Theoretical study of statistical fractal model with applications to mineral resource prediction. Comput. Geosci. 28, 369–376.
Sillitoe, R.H., 1997. Characteristics and controls of the largest porphyry copper-gold and epithermal gold deposits in the circum-pacific region. Aust. J. Earth Sci. 44, 373–388.
Sillitoe, R.H., 2002. Some metallogenic features of gold and copper deposits related to alkaline rocks and consequences for exploration. Miner. Deposita 37, 4–13.
Sim, B.L., Agterberg, F.P., Beaudry, C., 1999. Determining the cutoff between background and relative base metal contamination levels using multifractal methods. Comput. Geosci. 25, 1023–1041.
Simmons, S.F., White, N.C., John, D.A., 2005. Geological Characteristics of Epithermal Precious and Base-metal Deposits. Economic Geology 100th Anniversary Volume, pp. 485–522.
Stocklin, J., 1968. Structural history and tectonics of Iran: a review. AAPG Bulletin 52, 1229–1258.
Turcotte, D.L., 1986. A fractal approach to the relationship between ore grade and tonnage. Econ. Geol. 18, 1525–1532.
White, N.C., Hedenquist, J.W., 1995. Epithermal gold deposits: styles, characteristics and exploration. SEG Newsletter 23, 1–14.
Zuo, R., 2011a. Identifying Geochemical Anomalies Associated with Cu and Pb-Zn Skarn Mineralization Using Principal Component Analysis and Spectrum-Area Fractal Modelling in the Gangdese Belt, Tibet (China). J. Geochem. Explor. 111, 13–22.
Zuo, R., 2011b. Decomposing of mixed pattern of arsenic using fractal model in Gangdese belt, Tibet, China. Appl. Geochem. 26, S271–S273.
Zuo, R., Cheng, Q., Agterberg, F.P., Xia, Q., 2009a. Application of singularity mapping technique to identification local anomalies using stream sediment geochemical data, a case study from Gangdese, Tibet, western China. J. Geochem. Explor. 101, 225–235.
Zuo, R., Cheng, Q., Xia, Q., 2009b. Evaluation of the uncertainty in estimation of metal resources of skarn tin in southern China. Ore Geol. Rev. 35, 415–422.
Zuo, R., Cheng, Q., Xia, Q., Agterberg, F.P., 2009c. Application of fractal models to distinguishing between different mineral phases. Math. Geosci. 41, 71–80.
Zuo, R., Cheng, Q., Xia, Q., Agterberg, F.P., 2009d. Application of fractal models to characterization of vertical distribution of geochemical element concentration. J. Geochem. Explor. 102, 37–43.